EAN 2024 62nd annual conference on experimental stress analysis

Methodology and Determination of Parameters for Modeling Brittle Adhesive

L. Horák[1,*], J. Krystek[1]

[1] *Department of Mechanics, Faculty of Applied Sciences, University of West Bohemia, Univerzitní 8, 301 00 Pilsen, Czech Republic*

[*] *horakl@kme.zcu.cz*

Abstract: In the numerical simulation of adhesive joints, a significant challenge lies in obtaining reliable experimental data due to the wide variety of adhesives available, each with distinct material properties and different material models. This study focused on testing the methodology for obtaining mechanical parameters using bulk adhesive specimens. The experiments were conducted on a brittle adhesive, specifically Araldit AV 138+HY 998, which was selected as a representative material for structural adhesives. The study also evaluated fracture parameters, including the strain energy release rate, an essential parameter for predicting the fracture behavior of adhesive joints. By focusing on a specific adhesive material, this study aimed to obtain its mechanical parameters and use them in numerical simulations.

Keywords: Adhesive; Mechanical testing; Bulk specimen; DCB; ENF.

1 Introduction

Mechanical testing of adhesives is crucial in ensuring bonded assemblies' reliability and durability. Bulk specimens are commonly used for this purpose, as they provide a convenient and standardized way to measure the mechanical properties of adhesives.

Bulk specimens are typically prepared by casting or molding the adhesive into a standardized shape, such as a dog–bone or cylinder. The specimen is then subjected to various mechanical tests, including tensile, compression, and shear tests. These tests measure the stress-strain behavior of the adhesive, which is used to calculate important mechanical properties such as the modulus of elasticity, yield strength, and ultimate tensile strength. [1]

One of the main advantages of using bulk specimens for mechanical testing is that they allow for measuring the adhesive's properties independent of the substrate material. This is important because the substrate material can influence the mechanical properties of the adhesive, and testing the adhesive alone provides a more accurate measure of its intrinsic properties.

However, it is essential to note that the mechanical properties of bulk specimens may not always correlate directly with the performance of the adhesive in real-world applications. This is because the mechanical behavior of adhesives can be influenced by various factors, including the surface preparation of the substrate, the thickness and geometry of the bond line, and the environmental conditions during application and use. [2]

To address these challenges, researchers have developed a range of advanced testing methods that can more accurately simulate the conditions experienced by adhesives in real-world applications. These methods include dynamic mechanical analysis, fracture mechanics testing, and environmental testing.

All these parameters are then applicable to associated material models in numerical simulations, which, with suitable criteria for adhesive failure, can determine safe loads and the duration of these loads. [3]

2 Experiments

The thixotropic paste adhesive Araldit AV 138, with hardening component HY 998, was selected as a representative of structural brittle adhesives. It is a two-component epoxy–based adhesive that cures at room temperature and is considered appropriate for high-strength use in aggressive or warm environments. A series of experiments were conducted to obtain the mechanical parameters specified in Table 1, where appropriate parameters and tests are associated. [5] All experiments were conducted using the Zwick/Roell Z050 universal testing machine (UTM) equipped with a 50 kN load cell. The tests were performed at an ambient temperature of 23 ± 1°C, and the atmospheric moisture was within the range of $50 \pm 6\%$

Since the adhesive tested in this study is brittle and elastic, no mechanical parameters for plasticity were assumed. The experiments focused on determining the elastic, fracture initiation, and crack propagation parameters, which are critical for predicting the behavior of adhesive joints under various loads and conditions.

Tab. 1: Parameters for complex numerical simulation.

Zone name	Parameter name	Symbol	Unit	Experiment
Elastic	Young's modulus	E	[Pa]	Tensile test
	Poisson's ratio	ν	[-]	Tensile test
	Shear modulus	G	[Pa]	Arcan test
Iniciation of Fracture	Tensile failure strength	σ_{f}^{T}	[Pa]	Tensile test
	Shear failure strength	τ_{f}	[Pa]	Arcan test
	Tensile failure strain	$\epsilon_{\mathrm{f}}^{T}$	[-]	Tensile test
Crack propagation	Strain energy release rate for mod I	G_I	[Jm^{-2}]	DCB
	Strain energy release rate for mod II	G_{II}	[Jm^{-2}]	ENF

Bulk adhesive specimens were prepared for tensile, compression, and shear (Arcan) tests. To fabricate these specimens, a thin plate of adhesive was cast in a simple mold. During the mixing process, the two components were combined in an open container, which inevitably introduced air into the adhesive mixture. To mitigate this issue and ensure uniformity, the cast adhesive plate was subjected to a vacuum pump. The vacuum treatment was varied, with exposure times ranging from 2 to 25 minutes and negative pressures between -800 and -990 mbar. After the curing process at room temperature, selected samples underwent milling to achieve precise geometry and thickness tailored to the specific experimental requirements. The dimensions of the tensile and shear specimens are outlined in Fig. 1. The Arcan sample was configured to align with the fixtures in the Arcan test setup and facilitate fracture initiation from the tip [4]. In contrast, the tensile dog–bone test specimen was crafted to accommodate a biaxial extensometer with minimal height and dimensions.

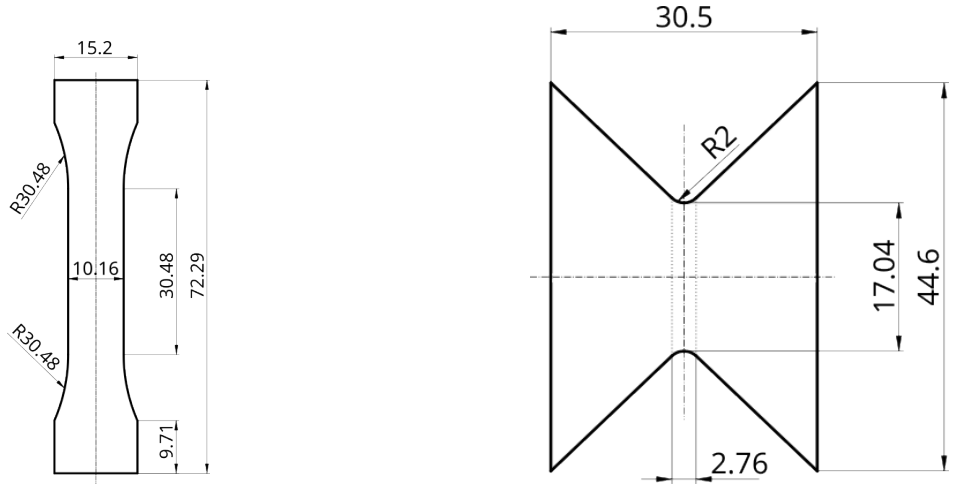

(a) Tensile sample

(b) Shear (Arcan) sample

Fig. 1: Geometry [mm] of samples used in tensile and shear experiments.

Double cantilever beam (DCB) and end-notched flexure (ENF) tests were performed to evaluate crack propagation parameters. DCB samples were made from two aluminum prismatic strips with dimensions $150 \times 20 \times 2$ mm, all dimensions are outlined in Fig. 2 (a). The prismatic strip surface was roughened with sandpaper and cleaned with an acetone-based cleaner. Initial delamination was $a_0 = 65$ mm. Load transfer was done through loading blocks, which were bonded to the specimen by the same adhesive. For one batch of samples, the specimens were placed in a vacuum chamber for 10 minutes with a running vacuum pump. This procedure aimed to assess the possibility of removing all air bubbles without altering the material properties of the adhesive.

ENF samples were made from two steel prismatic strips with dimensions $150 \times 20 \times 3$ mm, all dimensions are outlined in Fig. 2 (b). The prismatic strip surface was prepared as DCB samples. Initial delamination was $a_0 = 55$ mm. For correctly evaluating the propagation of the crack, it is crucial that any residual adhesive on the side was removed and the side was cleaned. If sandpaper is used, it is recommended that the sample be sanded in a perpendicular direction before testing. The change in material from aluminum to steel is due to the larger shear stress on the adhesive and the increased plastic deformation of the adherend.

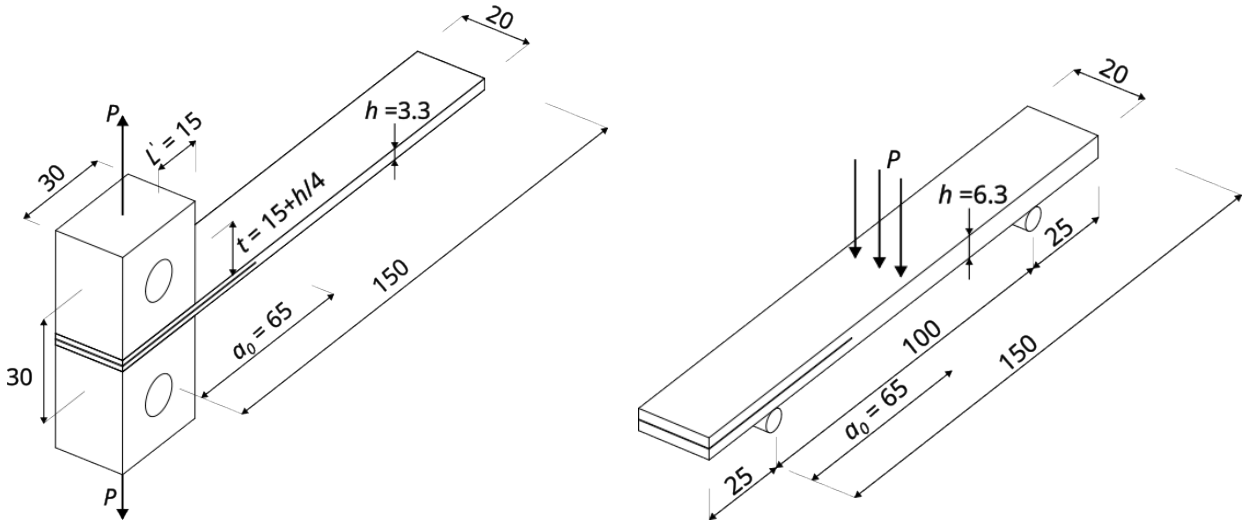

(a) DCB sample

(b) ENF sample

Fig. 2: Geometry [mm] of samples used in DCB and ENF experiments.

2.1 Tensile Experiments

For evaluating Young's modulus E, Poisson's constant ν, and ultimate tensile stress σ_{f}^{T}, tensile samples were loaded with prescribed constant crosshead rate $v_T = 1$ mm/min.

In total, 11 specimens were tested, which differed in thickness h from 1 to 3 mm and slight deviation when fabricating the base plate to eliminate air in the mixture. The Young's modulus was evaluated on a range of longitudinal strain values (ϵ_L) between 0.005 and 0.015, using data from 11 test specimens. Tensile failure strength was evaluated on seven samples. The remaining samples had visible air bubbles in place of the fracture. Poisson constant was measured with a biaxial extensometer and evaluated on the same longitudinal strain ϵ_L from 0.005 to 0.015 as Young's modulus. Five samples were utilized for this evaluation. The fracture was observed in the gauge section and out of the biaxial extensometer fixture. By this, the shape and dimensions of the tensile specimen were validated. Stress–Strain curve is on Fig. 3 (b).

Due to different ways of manufacturing the adhesive plate, it was observed that some of the samples had air bubbles in place of fracture, which prematurely initiated the fracture. This was visually inspected after the test and is visible in Fig. 3 (a). These samples had approximately 35 % lower failure strength. Many samples exhibiting high failure strength did not display a completely homogeneous structure along their fracture path.

2.2 Arcan Experiments

The Arcan samples were loaded at a prescribed constant crosshead rate of $v_{Arc} = 1$ mm/min. The samples were positioned at the center using 3D–printed plates and secured to the Arcan fixture using clamps tightened

(a) Photograph of fractured sample with non–uniform structure

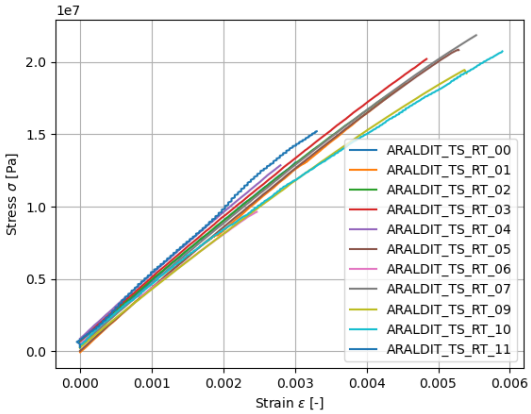

(b) Force–displacement curve for tensile experiment

Fig. 3: Tensile experiment.

by bolts. The bolts were screwed with a controlled torque of $M = 5$ N/m. The arcan experiment was performed to evaluate shear failure strength.

Force–displacement curve is on Fig. 4 (b), with visualization of fractured sample in the fixture on Fig. 4 (a). Accurate displacement was not measured, and the shear modulus was computed using Young's modulus and Poisson's constant.

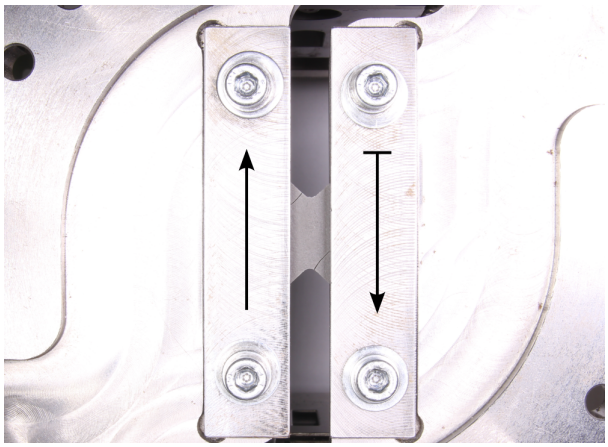

(a) Arcan sample in UTM fixture with visible cracks

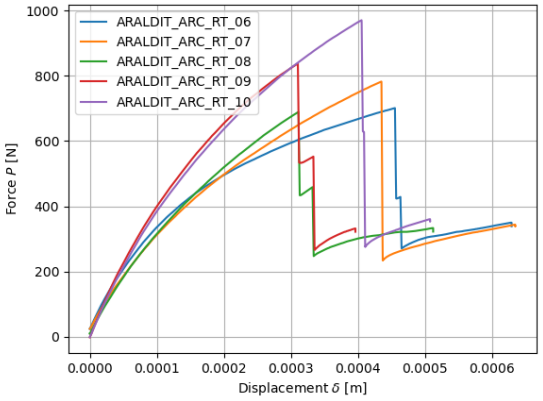

(b) Force–displacement curve

Fig. 4: Arcan experiment.

An adhesive crack initiated as expected at the location of the smallest cross-section of the sample. However, the crack propagated further to the sample. This unexpected crack propagation may have been caused by the presence of air bubbles in the adhesive. In all test specimens, two cracks were observed to form nearly simultaneously at the point of failure. The formation of these two cracks is evident in the Force–displacement curve recorded during testing.

2.3 Compression Experiments

The compression experiments were performed according to standard ASTM D695. Compression samples were loaded with prescribed constant crosshead rate $v_C = 1$ mm/min. Samples were milled from the same plate as shear and tension samples. Cylindrical samples with approximate dimensions $h = 4.8$ mm and radius $d = 12.4$ mm were used. This experiment was performed to evaluate compression failure strength. Force–displacement curve is on Fig. 5 (b).

Specimens with numbers 01 and 02 had visible air bubbles on the side of the specimen, as visible in Fig. 5 (a). The rest seems without any defect. Excluding the first specimen, the compression failure strength remained

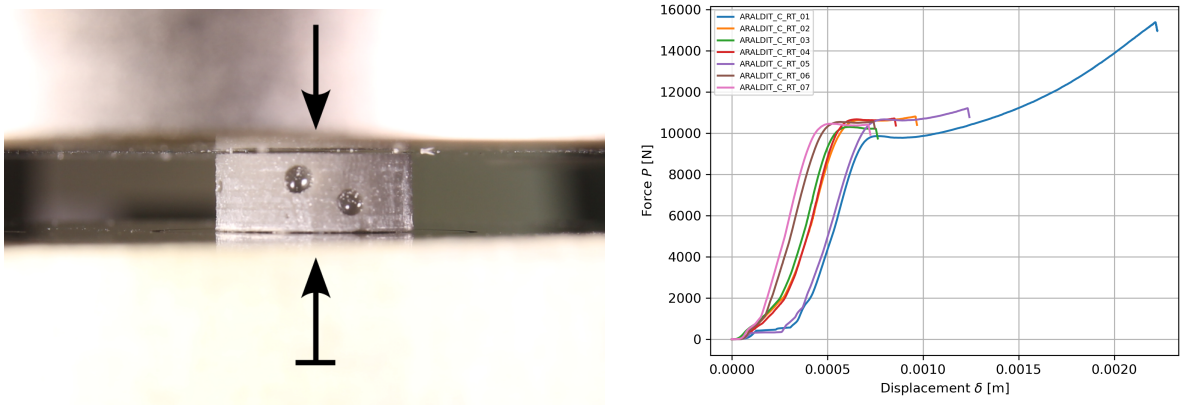

(a) Compression sample in UTM

(b) Force–displacement curve

Fig. 5: Compression experiment.

consistent across all measured specimens. The first specimen, numbered 01, was measured beyond the failure, while the remaining samples were measured until the first force drop occurred.

2.4 DCB Experiments

DCB experiments were performed according to standard ASTM D5528-01. The specimen was loaded with a constant crosshead rate $v_{\mathrm{DCB}} = 10$ mm/min. All samples were fractured cohesively, corresponding with the expected fracture mode. For further evaluation, adhesive fracture toughness for mode I was computed according to the modified beam theory as

$$G_I = \frac{3P\delta}{2B(a + |\Delta|)}, \tag{1}$$

where P is applied load during crack propagation with crack length a, δ is load point displacement, B is the width of the specimen, and Δ is a term for correction due to possible rotation, which may be determined experimentally by generating a least squares plot of the cube root of compliance as a function of delamination length.

Due to the use of loading blocks that have pins further from the top face of the specimen, correction due to stiffening is needed. Correction is computed as

$$N = 1 - \left(\frac{L'}{a}\right)^3 - \frac{9}{8}\left[1 - \left(\frac{L'}{a}\right)^2\right]\left(\frac{\delta t}{a^2}\right) - \frac{9}{35}\left(\frac{\delta}{a}\right)^2, \tag{2}$$

where L' is the distance from the loading pin to the end of the block in the direction to the opposite end of the sample, and t is the distance from the pin to the top face of the sample. To this distance, $h/4$ is added. These parameters are characterized on Fig. 2 (a). The correction is applied to compliance C as C/N when plotting compliance versus crack length. The crack length was measured from synchronized photographs taken during measurements.

In total, nine samples were tested, where samples from 1–4 were bonded without any additional steps, and samples 5–9 were let in a vacuum chamber with a vacuum pump continuously running. Force–displacement curves and R–curve for DCB are on Fig. 6 .

The 5% offset evaluation was not employed for the adhesive as it yielded overly conservative values. Fracture energy was determined from the R-curve in the region where crack propagation was initiated. It is evident that there are distinct differences in further crack propagation and fracture energy between the batch left in the vacuum pump and the others. This discrepancy warrants further investigation.

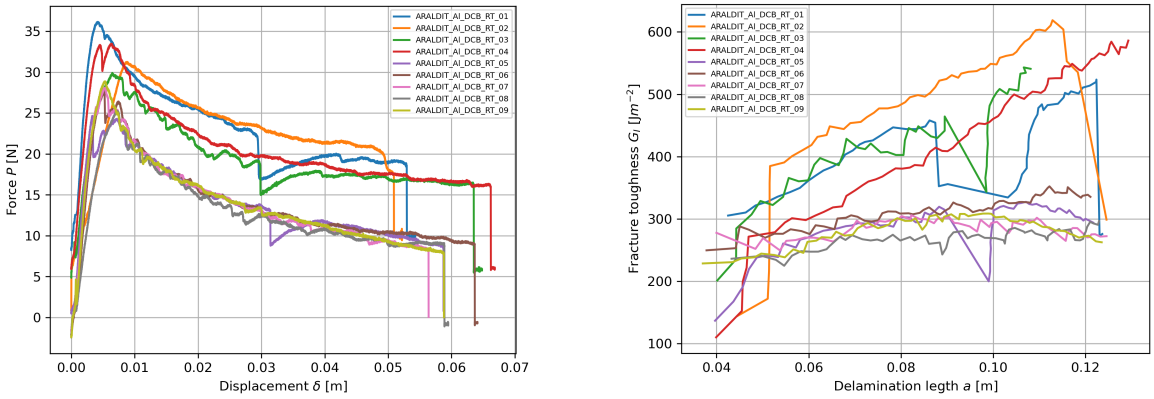

(a) Force–displacement curves

(b) R–curves

Fig. 6: Results of DCB experiments.

2.5 ENF Experiments

ENF experiments were performed according to standard ASTM D7905. The loading of the specimen was carried out with a constant crosshead rate $v_{\text{ENF}} = 0.5$ mm/min. Crack length was measured as in DCB from synchronized photographs. For further evaluation, adhesive fracture toughness for mode II was computed as

$$G_{II} = \frac{3mP_{\text{max}}^2 a_0^2}{2B}, \tag{3}$$

where P_{max} is applied load during crack propagation with initial crack length a_0. δ is load point displacement, B is width of specimen and m is term of compliance calibration coefficients. Determined using a linear least squares regression analysis of the compliance C versus crack length cubed a^3.

Force–displacement curves are shown in Fig. 7 (a) and the R–curve for ENF, which represents Mode II interlaminar fracture toughness on delamination length on Fig. 7 (b). The black $\times$ marks on the Force–displacement curves indicates the recorded crack length.

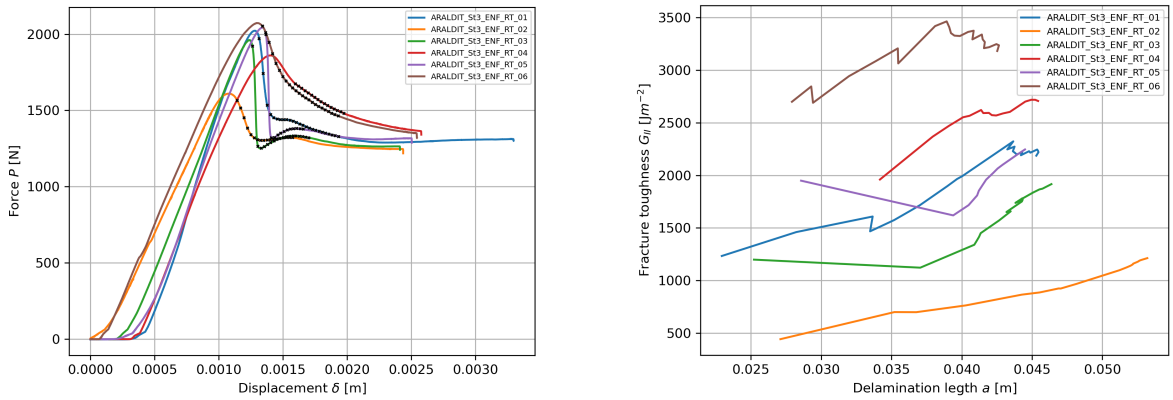

(a) Force–displacement curves

(b) R–curves

Fig. 7: Results of ENF experiments.

The significant variation in results may be attributed to the thicker adhesive layer, which, when compressed during the curing process, formed rounded ends that propagated unexpectedly. This might be one of the causes. Based on these findings, it is recommended to reduce the crosshead rate when testing stiffer and thicker materials. Additionally, during fabrication, it is crucial to verify that the insert is positioned correctly and that the adhesive is not flowing around it to ensure accurate results.

3 Results

From the above experiments, material parameters were evaluated with values summarized in Table 2. The standard deviation was computed for the sample and not the whole population. CV in the table is an abbreviation for the coefficient of variation. Shear modulus was computed from Young's modulus and Poisson's constant.

Tab. 2: Evaluated parameters for complex numerical simulation.

Property	Symbol	Unit	Average	Standard deviation	CV [%]
Young's modulus	E	[GPa]	4.17	0.25	6.00
Poisson's ratio	ν	[–]	0.44	0.03	6.82
Shear modulus	G^*	[GPa]	1.45	–	–
Tensile failure strength	σ_{f}^T	[MPa]	19.91	1.43	7.18
Tensile failure strain	ϵ_{f}^T	[%]	0.51	0.05	9.80
Compression failure strength	σ_{f}^C	[MPa]	90.42	5.37	5.94
Shear failure strength	τ_{f}	[MPa]	16.67	1.91	11.46
Strain energy release rate for mod I	G_I	[Jm^{-2}]	292.78	52.72	18.01
Strain energy release rate for mod II	G_{II}	[Jm^{-2}]	1704.2	850.95	49.93

4 Conclusion

This work summarizes the methodology for obtaining complex mechanical parameters for brittle adhesives and measures these parameters for adhesive Araldit AV 138+HY 998.

Several experiments were conducted for the elastic zone parameters, including Young's modulus in tension, Poisson's constant, and Young's modulus in shear, including tensile tests, extensometer measurements, and Arcan tests. The evaluation of these parameters exhibited a low coefficient of variation, confirming the validity of the testing methodology.

The fracture initiation parameters, including tensile stress limit, compressive stress limit, shear stress limit, and ultimate tensile deformation, were assessed through tensile tests, compression tests, and Arcan tests. The tensile test revealed sensitivity to the manufacturing process of the adhesive plate. When air bubbles were present in the mixture, the tensile failure strength decreased by 35% compared to samples where the fracture occurred in areas without air bubbles.

To evaluate crack propagation parameters such as the strain energy release rate for modes I and II, specimens were prepared for Double Cantilever Beam (DCB) and End-Notched Flexure (ENF) tests. The DCB test was successfully validated for methodology but revealed uncertainty in the handling of the vacuum pump. The ENF test highlighted weaknesses in the current adhesive testing methodology.

Acknowledgement

This research work was supported by the project SGS-2022-008.

References

[1] A.M.G. Pinto et al., Shear Modulus and Strength of an Acrylic Adhesive by the Notched Plate Shear Method (Arcan) and the Thick Adherend Shear Test (TAST), Materials Science Forum 636-637 (2010) 787–792, doi: 10.4028/www.scientific.net/MSF.636-637.787.

[2] M.D. Banea, L.F.M da Silva, Adhesively bonded joints in composite materials: An overview, Proceedings of the Institution of Mechanical Engineers, Part L: Journal of Materials: Design and Applications 223 (2009) 1–18, doi: 10.1243/14644207JMDA219.

[3] G. Dean, B. Duncan, Preparation and Testing fo Bulk Specimens of Adhesives, Teddington, Middlesex, National Physical Laboratory, 1998, ISSN 1368-6550.

[4] R. Kotner, J. Heczko, J. Krystek, Validation of identified material parameters of rubber using an Arcan shear test, Materials Today: Proceedings 12(2) (2019) 404–410, doi: 10.1016/j.matpr.2019.03.142.

[5] E. M. Petrie, Handbook of Adhesives and Sealants, New York, USA, MCGraw-Hill, 2000.